ACS Catalysis

Research Article

pubs.acs.org/acscatalysis

Alcohol Amination with Aminoacidato Cp*Ir(III)-Complexes as Catalysts: Dissociation of the Chelating Ligand during Initiation

Simone Wöckel,[†] Philipp Plessow,[†,‡] Mathias Schelwies,[§] Marion K. Brinks,[§] Frank Rominger,[∥] Peter Hofmann,[†,∥] and Michael Limbach*[,†,§]

[†]CaRLa (Catalysis Research Laboratory), Im Neuenheimer Feld 584, 69120 Heidelberg, Germany

[‡]Quantum Chemistry and [§]Synthesis & Homogenous Catalysis, BASF SE, Carl-Bosch-Strasse 38, 67056 Ludwigshafen, Germany

[∥]Organisch-Chemisches Institut, Ruprecht-Karls-Universität Heidelberg, Im Neuenheimer Feld 270, 69120 Heidelberg, Germany

Supporting Information

ABSTRACT: The use of aminoacidato Cp*Ir(III)-complexes in catalytic alcohol amination reactions of primary and secondary alcohols with amines permits to carry out these transformations at very mild reaction conditions without the use of an additional base. Herein we discuss the fate of the chelating aminoacidato ligands upon initiation of Cp*Ir(III)-complexes from a mechanistic perspective. Catalyst initiation has been followed by NMR using isotopically labeled ^{13}C,^{15}N-glycinato complexes.

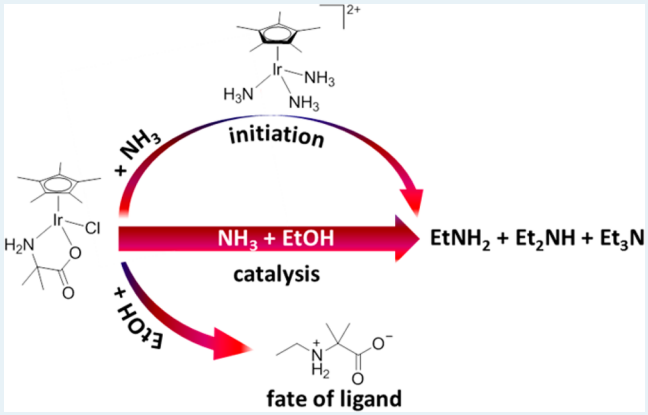

KEYWORDS: *alcohol amination, hydrogen borrowing, iridium, sandwich complexes, amino acids*

INTRODUCTION

The catalytic amination of alcohols is an atom-economical synthetic route to primary, secondary, or tertiary amines from readily available starting materials.[1] State-of-the-art catalysts for the synthesis of amines from ammonia and alcohols on a large scale are Brønstedt-acidic and heterogeneous in nature. Homogenous catalysts supplement the heterogeneous catalysts in a useful way since they work at milder reaction conditions with respect to temperature. Additionally, an intrinsically different reaction pathway, that is, a hydrogen borrowing mechanism (Scheme 1) as opposed to nucleophilic substitution, allows a more selective access to more complicated amines. In industrial process development in the area of fine-chemicals[2] besides complexes based on ruthenium[3] and other transition metals,[4] especially iridium complexes[5] turned out to be highly active and selective catalysts to generate secondary or tertiary amines from an alcohol and an amine source. Examples are Fujita's and Yamaguchi's $[Cp^*IrCl_2]_2$ (**1**)[6] and $[Cp^*Ir(NH_3)_3]\cdot 2I$ (**2**), iridium(III)-NHC-complexes of Crabtree[7] and Peris[8] (e.g. **3**, cf. Scheme 1) or just $[Ir(COD)Cl]_2$ in combination with a phosphine-ligand.[9]

Especially the air-stable tris(ammine) complexes $[Cp^*Ir(NH_3)_3]X_2$ (X = I, Br, Cl) reported by Fujita and Yamaguchi enable the selective formation of secondary or tertiary amines in water.[10] The activity of **2** is superior to its halide derivatives, and all complexes tolerate a broad scope of substrates without the need of basic additives.[11] [Cp*Ir(Pro)Cl] (**4**) and similar Cp*Ir(III)-complexes bearing chelating aminoacidato ligands[12] do not require bases, either, and allow for even milder reaction conditions than literature paragons **1** and **2** (T < 100 °C). Their substrate and functional group tolerance in organic solvents *as well as* in water is broad. Surprisingly, although iridium(III) half-sandwich complexes bearing α-,[13] β-aminoacidato,[14] or even peptide-derived ligands[15] have been known for decades, their application in catalysis, for example, alcohol amination or asymmetric transfer hydrogenation, is just emerging.[12,16] From the mechanistic point of view, those catalysts are far less explored.[6,11] This motivated us to investigate how complexes with aminoacidato ligands such as **4** initiate and what the fate and relevance of the aminoacidato ligand is under catalytic conditions. Consequently, we synthesized aminoacidato Cp*Ir(III)-complexes **4** to **11** (Scheme 2) to investigate the role of their aminoacidato ligands under reaction conditions using NMR spectroscopy. To further investigate the activity determining structural features of the catalyst, we also studied the influence of the halide ligand at the iridium center on catalytic activity and selectivity.

Received: October 17, 2013
Revised: November 28, 2013
Published: December 3, 2013

   dx.doi.org/10.1021/cs4009418 | *ACS Catal.* 2014, 4, 152−161

Scheme 1. Proposed Hydrogen Borrowing Mechanism and Pre-Catalysts 1−4

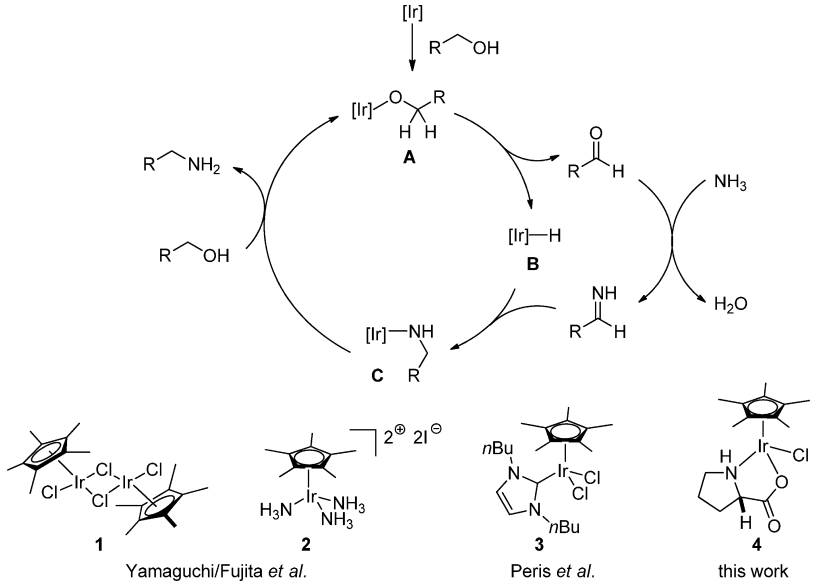

Scheme 2. Synthesis of Complexes 4 and 6−11

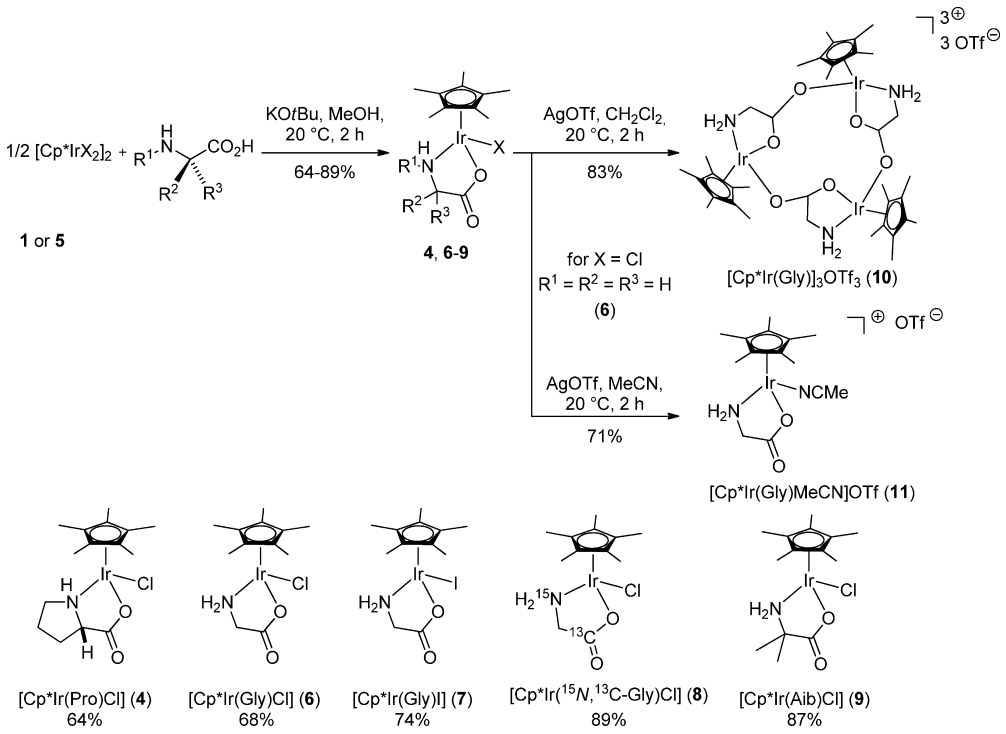

RESULTS AND DISCUSSION

Synthesis of Complexes 4 and 6−11. A suspension of $[Cp^*IrCl_2]_2$ (**1**)[17] or $[Cp^*IrI_2]_2$ (**5**),[18] the appropriate amino acids glycine (Gly), (*S*)-proline (Pro) or aminoisobutyric acid (Aib) and potassium *tert*-butoxide (KO*t*Bu) in methanol was reacted at room temperature for 2 h. After a workup sequence of filtration and recrystallization from CH_2Cl_2 layered with excess pentane, complexes **4** and **6−9** were isolated in good yields as yellow or orange crystals (64−89%, Scheme 2).

Surprisingly, when we aimed to synthesize a complex without a direct halide substituent on the iridium center of the catalyst using silver triflate (AgOTf) to remove the halide, trimer $[Cp^*Ir(Gly)]_3(OTf)_3$ (**10**) was obtained in 83% yield from **6**. X-ray structure analysis revealed the saturation of the vacant coordination side at iridium by the exocyclic oxygen atom of the aminoacidato ligand of a second iridalactone (Figure 1). Such trimeric metallalactones with other aminoacidato ligands than glycinato have been already reported by Carmona et al.[16] and others.[13d,19] When **6** and AgOTf were reacted in a coordinating solvent such as acetonitrile (MeCN), [Cp*Ir-(Gly)MeCN]OTf (**11**) was formed and isolated in 71% yield.

Crystals of [Cp*Ir(Gly)I] (**7**) as well as the acetonitrile complex [Cp*Ir(Gly)MeCN]OTf (**11**), both complexes bearing the achiral κ^2-N,O-glycinato ligand, were obtained either by slow crystallization from CH_2Cl_2 layered with pentane or from MeCN/Et_2O (Figure 1). Complex **7** crystallized with

dx.doi.org/10.1021/cs4009418 | ACS Catal. 2014, 4, 152−161

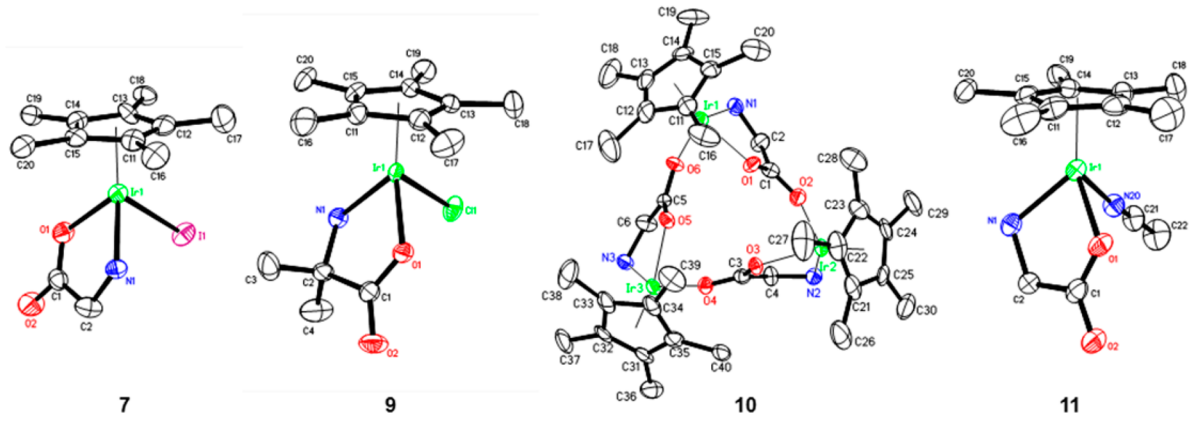

Figure 1. Solid state (X-ray) molecular structures of [Cp*Ir(Gly)I] (**7**), [Cp*Ir(Aib)Cl] (**9**), $[Cp^*Ir(Gly)]_3(OTf)_3$ (**10**), and [Cp*Ir(Gly)-MeCN]OTf (**11**) with ellipsoids drawn at the 50% probability level. H atoms are omitted for clarity. Selected bond lengths and angles: **7** (two independent molecules): Ir–I 2.7182(6)/2.7015(8) Å, Ir–O 2.115(5)/2.115(6) Å, Ir–N 2.122(6)/2.134(6) Å, I–Ir–O 86.97(15)/87.07(16)°, I–Ir–N 86.89(17)/85.84(18)°, O–Ir–N 78.1(2)/78.0(2)°. **9** (two independent molecules): Ir–Cl 2.4100(14)/2.4174(15) Å, Ir–O 2.086(3)/2.088(4) Å, Ir–N 2.115(4)/2.126(4) Å, Cl–Ir–O 85.30(11)/85.53(12)°, Cl–Ir–N 82.56(13)/82.89(14)°, O–Ir–N 78.37(14)/77.89(15)°. **10**: Ir1–O6 2.116(6) Å, Ir1–O1 2.127(6) Å, Ir1–N1 2.110(8) Å, Ir2–O2 2.120(7) Å, Ir2–O3 2.125(5) Å, Ir2–N2 2.113(7) Å, Ir3–O4 2.146(6) Å, Ir3–O5 2.125(6) Å, Ir3–N3 2.124(7) Å, O1–Ir1–O6 84.3(3)°, O1–Ir1–N1 77.9(3)°, O6–Ir1–N1 80.2(3)°, O2–Ir2–O3 82.9(2)°, O2–Ir2–N2 79.1(3)°, O3–Ir2–N2 77.4(3)°, O4–Ir3–O5 82.8(2)°, O4–Ir3–N3 79.9(3)°, O5–Ir3–N3 77.5(3)°. **11**: Ir–N20 2.076(3) Å, Ir–O 2.105(3) Å, Ir–N1 2.117(3) Å, N20–Ir–O 85.02(12)°, N–Ir–N 85.23(13)°, O–Ir–N1 77.81(11)°.

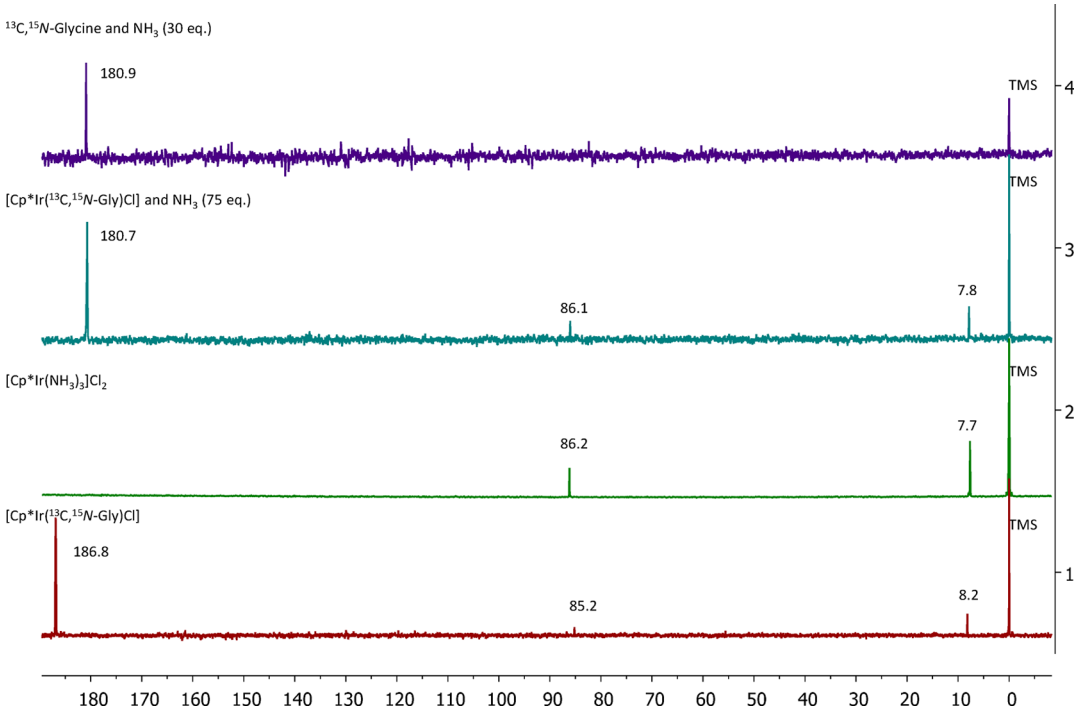

Figure 2. ^{13}C NMR spectra in D_2O of [Cp*Ir($^{13}C,^{15}N$-Gly)Cl] (**8**) (in red), [Cp*Ir(NH_3)$_3$]·2Cl (in green), **8** and NH_3 (in blue), and $^{13}C,^{15}N$-glycine and 30 equiv of NH_3 (in purple).

two independent molecules per unit cell, as did its chloro derivative [Cp*Ir(Gly)Cl] (**6**).[12] Because of its bigger size, the iodo ligand significantly elongated the metal-halide bond (2.7182(6)/2.7015(8) Å for **7** vs. 2.4177(6)/2.4143(7) for **6**), which goes along with a slight elongation of the Ir–O bond (2.115(5)/2.115(6) for **7** vs. 2.0992(18)/2.0998(18) for **6**). Change of the chloro ligand to the neutral donor acetonitrile does not significantly influence the geometry around iridium in [Cp*Ir(Gly)MeCN]OTf (**11**).

Mechanistic Studies. Although structurally very similar, the activity of complexes bearing aminoacidato ligands (cf. **7** and **6**) turned out to be sensitive to the substituent at the *α*-position and the N-terminus of the aminoacidato ligand.[12] This is why we investigated catalyst initiation and the influence of the aminoacidato ligand on reactivity more closely. For mechanistic studies complex **8** was used, the $^{13}C,^{15}N$-labeled glycinato ligand which provided an excellent spectroscopic handle to follow the course of the reaction and the fate of the aminoacidato ligand by NMR spectroscopy. Although a stoichiometric experiment using precatalyst [Cp*Ir($^{13}C,^{15}N$-Gly)Cl] (**8**), 1-octanol and gaseous NH_3 (ca. 60 equiv) demonstrated the poor solubility of **8** in the organic solvent d_8-

dx.doi.org/10.1021/cs4009418 | ACS Catal. 2014, 4, 152–161

Scheme 3. Reaction of 9 with a Slight Excess of aq. NH_3 Gives 12, whereas the Resting-State of Pre-Catalysts 1, 4, and 13 in the Presence of a Large Excess of NH_3 is 13

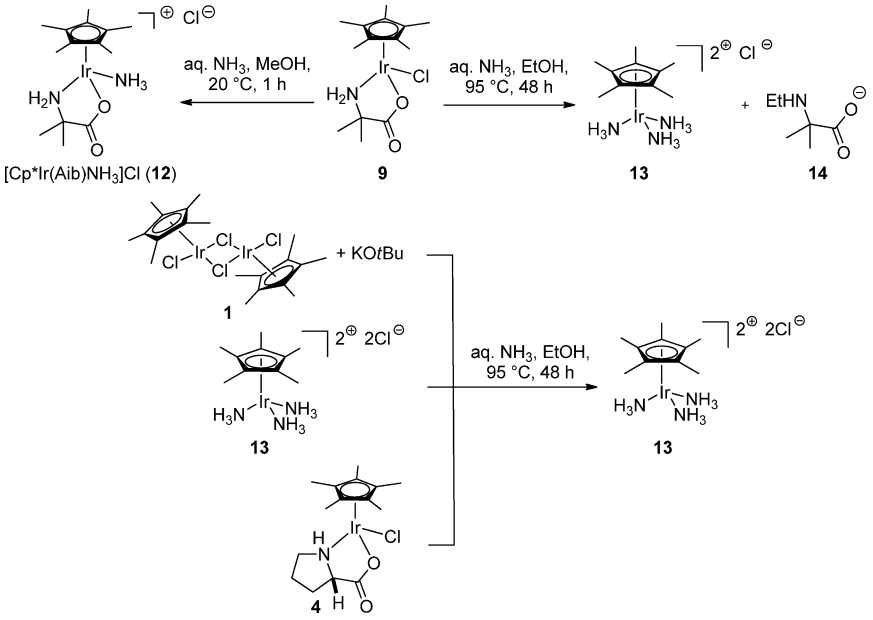

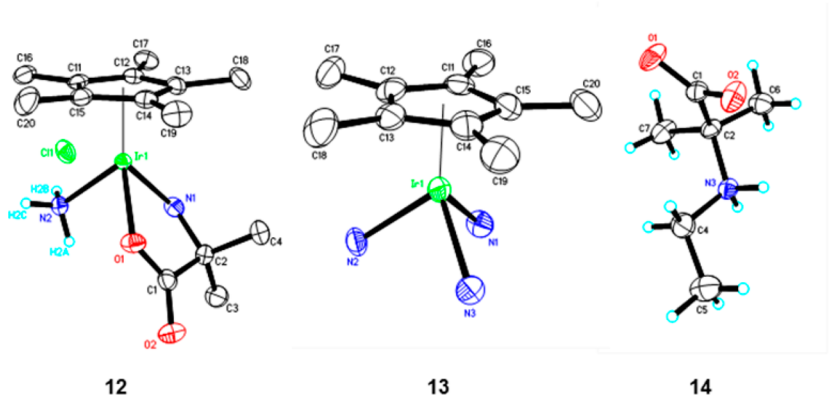

Figure 3. Solid state (X-ray) molecular structures of $[Cp^*Ir(Aib)NH_3]Cl$ (**12**), $[Cp^*Ir(NH_3)_3]Cl_2$ (**13**), and *N*-ethyl-aminoisobutyric acid (**14**), with ellipsoids drawn at the 50% probability level. Most H atoms are omitted for clarity. Selected bond lengths and angles: **12**: Ir−N2 2.123(3) Å, Ir−O1 2.110(2) Å, Ir−N1 2.133(3) Å, N2−Ir−O1 82.18(10)°, N2−Ir−N1 82.99(10)°, O1−Ir−N1 77.12 (10)°.

toluene even after heating the reaction mixture to 65 °C for 24 h, the color of the suspended solid changed from yellow to pale yellow. After decantation of the supernatant liquid, washing of the precipitate with Et_2O and a drying step, the ^1H NMR spectrum of this precipitate in d_4-MeOD revealed a singlet at δ = 1.74 ppm, which fits the shift of the Cp*-signals reported earlier by Yamaguchi et al. for the tris(ammine)-ligated complex $[Cp^*Ir(NH_3)_3]\cdot 2Cl$.[10]

Based on the stoichiometric reaction of **2** and benzyl alcohol (BnOH) in D_2O at 140 °C, Yamaguchi et al. reported as the initial steps of the catalytic cycle (cf. Scheme 1) the formation of iridium-alkoxide species **A**, which readily eliminates a β-hydrogen of the alkoxide moiety and already after 30 min formed benzaldehyde (18%) and iridium-hydride **B**. The latter was identified by its ^1H NMR shift at δ = −15.49 ppm.[10] When $[Cp^*Ir(^{13}C,^{15}N\text{-Gly})Cl]$ (**8**) was reacted with BnOH in D_2O at 95 °C no benzaldehyde signal was observed (see Supporting Information, Figure S25), whereas the reaction of $[Cp^*Ir(Gly)Cl]$ (**6**) with an 10-fold excess of $BnNH_2$ in MeCN (1 h at 20 °C) yielded a pale yellow solid after removal of volatiles and washing the residue with Et_2O. Four species were detected by HR-FAB MS based on the fragments at m/z = 402, 470, 509, and 764, that were assigned to be $[M\text{-}Cl]^+$, $[M\text{-}Gly\text{+}BnNH_2]^+$, $[M\text{-}Cl\text{+}BnNH_2]^+$, and $[M\text{-}Gly\text{+}3BnNH_2]^+$, respectively (cf. Supporting Information; M = $[Cp^*Ir(Gly)Cl]$). The assumption that not only the chloro but also the aminoacidato ligand dissociates upon catalyst initiation became obvious when a solution of **8** in D_2O was reacted with 75 equiv of gaseous NH_3 and the reaction was followed by ^{13}C NMR spectroscopy (Figure 2): The signal of the coordinated amino acid at δ = 186.8 ppm moved to δ = 180.7 ppm, which corresponds to the carboxylate carbon of free $^{13}C,^{15}N$-Gly. At the same time, the diagnostic signals of the Cp* ligand shifted from δ = 85.2 ppm for **8** to 86.1 ppm, which is close to the corresponding resonance at δ = 86.2 ppm for $[Cp^*Ir(NH_3)_3]\cdot 2Cl$. The ^{15}N-spectra in D_2O point to the same conclusion as the signals of the coordinated amino acid shift from δ = −16.6 ppm to 28.1 ppm, which corresponds to the deprotonated, uncoordinated aminoacid anion.

dx.doi.org/10.1021/cs4009418 | ACS Catal. 2014, 4, 152−161

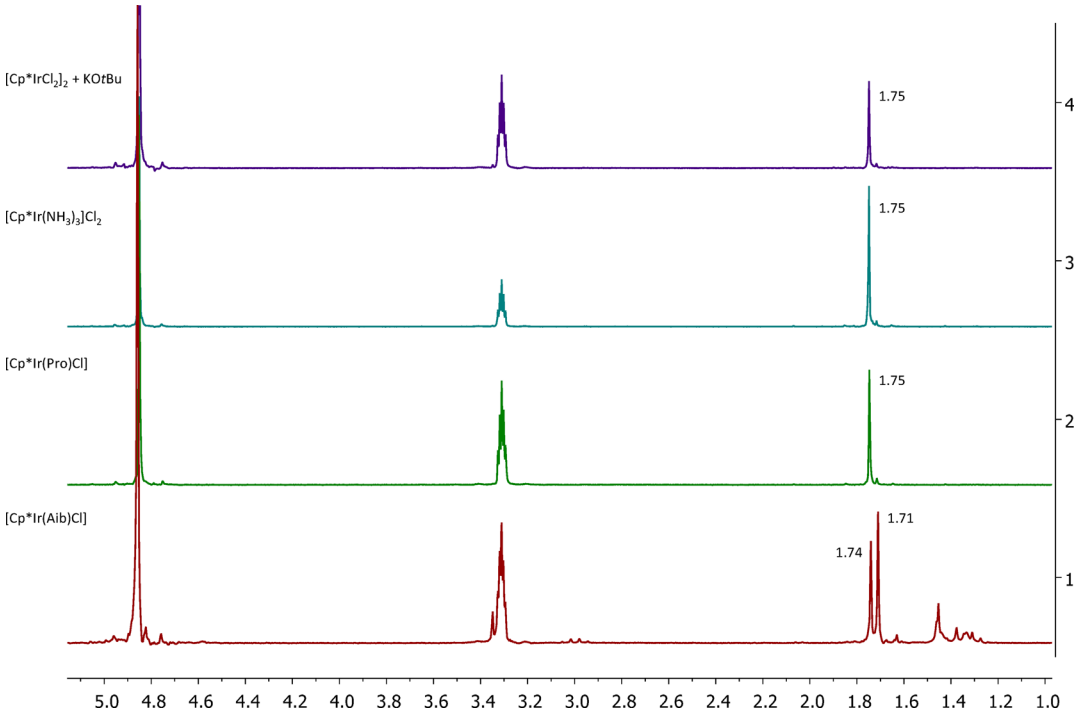

Figure 4. ^{1}H NMR spectra of the solutions of residues in d_4-MeOD obtained after the reactions of NH_3 with EtOH using **1** and KO*t*Bu (in purple), **13** (in blue), **4** (in green), and **9** (in red).

To prove this hypothesis [Cp*Ir(Aib)Cl] (**9**) was treated with 6 equiv of aq. NH_3 in MeOH (Scheme 3). Again, the color of the solution turned from bright to pale yellow. Removal of the solvent after 1 h at 20 °C and recrystallization of the residue from MeOH/Et_2O yielded single crystals of **12**. Here, the aminoacidato backbone still coordinates to iridium but obviously a ligand exchange of chloro to the neutral ammonia ligand has occurred (cf. Figure 3).

The bond lengths of **12** and **11**, both cationic complexes with a neutral N-donor ligand, turned out to be very similar, whereas the angles formed by the N-donor, iridium, and the O-terminus of the aminoacidato ligand are slightly smaller for **12** (N−Ir−O 82.18(10)°) vs. **11** (N−Ir−O 85.02(12)°).

Independent of the starting complex, that is, $[Cp^*IrCl_2]_2$, $[Cp^*Ir(NH_3)_3]Cl_2$, [Cp*Ir(Pro)Cl], or [Cp*Ir(Aib)Cl], the reaction with NH_3 and EtOH (48 h at 95 °C) yielded Yamaguchi's catalyst **13** as the final product (Scheme 3). It was unambiguously identified by X-ray analysis (Figure 3) or ^{1}H NMR spectroscopy (Figure 4) after removal of volatiles from the crude reaction mixture under reduced pressure and crystallization of the residue from MeOH/Et_2O. Furthermore, when **9** was used as catalyst, crystals of the N-alkylated aminoacid Aib were obtained. We consider these results as the ultimate proof that upon exposure to ammonia Yamaguchi's catalyst forms as a catalyst resting state.

Our experimental findings suggest a simple, thermodynamically favored ligand exchange upon catalyst initiation. Nevertheless, we decided to take a closer look at the initiation mechanism leading from complex [Cp*Ir(Gly)Cl] (**6**) to Yamaguchi's catalyst $[Cp^*Ir(NH_3)_3]^{2+}$ (**13**) by quantum chemistry using the density functional theory (DFT) methodology. The main uncertainty of such a computational investigation is the influence of solvation, since the reaction involves two charge separations. The influence of the method for electronic energies was found to be small: B3LYP-D3/def2-TZVP and M06/def2-TZVP[20] give basically identical results. With geometries obtained at the BP86/def2-SV(P) level of theory[21] using the RI approximation and suitable auxiliary basis sets,[22] we computed gas-phase free energies at p = 1 bar and T = 298.15 K within the usual rigid-rotator, harmonic oscillator, free translation approximation at the B3LYP-D3/def2-TZVP//BP86/def2-SV(P) level of theory with TURBOMOLE.[23] Gibbs free energies in water were obtained by adding free energies of solvation for water, ΔG_{solv}, resulting in free energies for infinite dilution at a reference concentration of 1 mol/L. The solvation free energies were computed with the SMD (M06/def2-TZVP) and COSMO-RS (BP86/def-TZVP) model.[24] The largest deviations between the solvation free energies computed this way were found for Cl^- ($\Delta\Delta G_{solv}$ = 96 kJ/mol) and the glycinato ligand ($\Delta\Delta G_{solv}$ = 66 kJ/mol). An experimental value is available for Cl^- ($\Delta G_{solv,exp}$ = −304 kJ/mol),[25] a good estimate for the anionic glycinato ligand ($\Delta G_{solv,exp}$ = −316 kJ/mol) is available from its experimental acidity in solution and in the gas-phase, $\Delta G_{solv,exp}$ of H^+ as well as a reasonably accurate calculation for ΔG_{solv} of glycine to either the neutral or the zwitterionic form (cf. Supporting Information for details). For these two examples, the values obtained (mainly) from experiment are bracketed by the computed ones (SMD/COSMO-RS). An experimental value is also available for NH_3 ($\Delta G_{solv,exp}$ = −10 kJ/mol).[26] These three experimental values for ΔG_{solv} have been employed in our calculations, all others have been obtained with COSMO-RS or SMD. The agreement of SMD and COSMO-RS for the neutral and positively charged metal complexes is fair; the deviation for Yamaguchi's complex **13** is only 5 kJ/mol. The largest remaining error of ΔG_{solv} is found for **6**, which is 34 kJ/mol more stable with COSMO-RS. We will discuss free energies at the B3LYP-D3/def2-TZVP//BP86/def2-SV(P) level in H_2O (c = 1 mol/L) with solvation free energies obtained as described above.

dx.doi.org/10.1021/cs4009418 | *ACS Catal.* 2014, 4, 152−161

Scheme 4. Ligand Exchange Reactions Yielding Yamaguchi's Complex 13 at the B3LYP-D3/def2-TZVP//BP86/def2-SV(P) Level in Water[a]

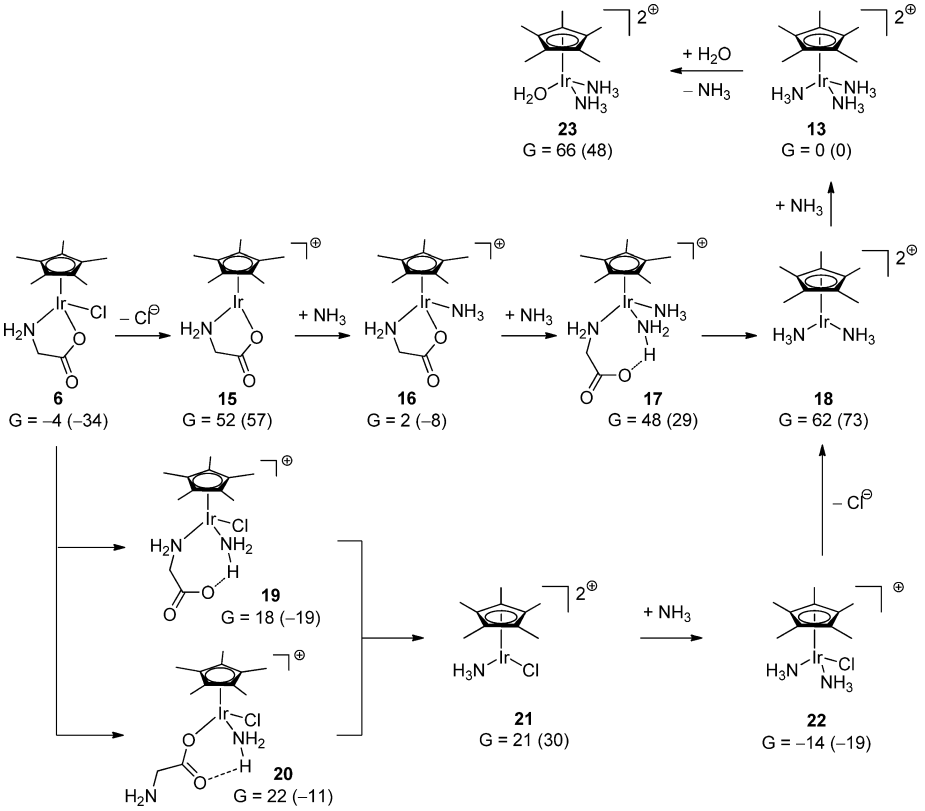

[a]The values in parentheses have been obtained with free energies of solvation computed with COSMO-RS and the others have been obtained with free energies of solvation computed with SMD. All free energies are given relative to **13**.

Initially, it is instructive to get an estimate of the experimental free reaction energy for **13**. An equilibrium ratio of **13** to **6** of 99:1 or higher means a maximal value of $\Delta G \leq +12$ kJ/mol (concentration of **6** of 0.06 mol/L, 60 equiv of NH_3). The computed results for the ligand-exchange reactions are presented in Scheme 4. We discuss all free energies relative to **13**. This way a high agreement between the two values for the computed solvation free energy with SMD or COSMO-RS has been achieved. In the backward reaction from **13** to **6**, the agreement of SMD/COSMO-RS is good for most of the reaction paths, and there are no high-energy intermediates that would hinder the reaction from occurring at room temperature. The most striking difference of the solvation models is the different stability of the precursor **6** (SMD: −4 kJ/mol and COSMO-RS: −34 kJ/mol). Both numbers bracket the value expected from experiment (≥−12 kJ/mol). The highest energy intermediate in the equilibrium is **18** (SMD: 62 kJ/mol; COSMO-RS: 73 kJ/mol).

Taking into account that SMD and COSMO-RS usually bracket the true value (where it is known) and that **6** is probably somewhat too low in free energy, we conclude that the dissociative ligand exchange pathway, cf. Scheme 4, accounts for the observed equilibrium between Ir-complexes with different ligands. Although those calculations do not allow to define a clear preference as to which ligand dissociates first starting from **6** via the coordinatively unsaturated (16-electron) complexes **15**, **18**, or **21** of flat geometry,[13g,h,27] our experimental findings based on the isolation of **12** point to an initial loss of the chloro ligand via **16**. The coordination geometry of the 16-electron complexes is flat (the plane defined by Ir and the two remaining "legs" of the piano stool is perpendicular to the Cp* ring-plane). This is in agreement with previous theoretical studies on this type of complexes.[27]

Catalysis. With the above-mentioned findings in mind and being aware of the significant differences in activity and selectivity for reactions catalyzed by Cp*Ir-complexes with different aminoacidato ligands in organic solvents,[12,28] we compared the performance of [Cp*Ir(Pro)Cl] (**4**) and $[Cp^*Ir(NH_3)_3]\cdot 2Cl$ (**13**) in the alkylation of benzylamine ($BnNH_2$) with benzyl alcohol (BnOH) to form dibenzylamine in toluene (Scheme 5, Table 1). The conversion obtained with

Scheme 5. Preparation of Dibenzylamine in Toluene[a]

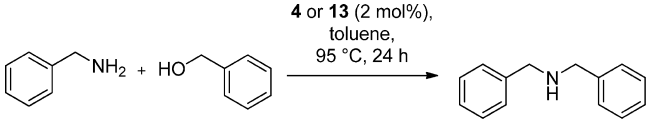

[a]For details, cf. Table 1.

4 was indeed significantly higher than that obtained with **13** (98 vs. 63%) at comparable selectivity. Furthermore, it turned out that **13** was not entirely soluble in toluene and solid material remained.

To ensure the complete solubility of the precomplexes in the reaction medium, we ran the reaction of $BnNH_2$ and 1,6-hexanediol in water to form N-benzylazepane (Scheme 6, Table 2). As expected from our findings concerning catalyst initiation,

dx.doi.org/10.1021/cs4009418 | ACS Catal. 2014, 4, 152−161

Table 1. Preparation of Dibenzylamine in Toluene

catalyst[a]	conv. (%)[b]	sel. (%)[c]
4	98	99
13	63	99

[a]Conditions: $BnNH_2$ (1 mmol), BnOH (1 mmol), toluene (0.3 mL), cat. (2 mol %), 95 °C, 24 h, diglyme (0.35 mmol as standard). Conversion and selectivity determined by GC analysis. [b]Conversion in $BnNH_2$. [c]Selectivity in dibenzylamine.

very similar conversion and selectivity was found for precomplexes **2**, **4**, **6**, **7** and **10**, **11**, **13**. The nature of the counterion (i.e., chloride, triflate) or halide ligand (i.e., chloro or iodo) had no effect on conversion and selectivity in water: This is in contrast to reports by Yamaguchi and Fujita.[10] When the Yamaguchi-type tris(benzylamino) complex **24** was formed in situ by stirring **6** with $BnNH_2$ in water for 3 h at 20 °C prior to addition of 1,6-hexanediol (Table 2 and Supporting Information), comparable conversion and selectivity to N-benzylazepane was observed.

In conclusion, we have shown that the aminoacidato ligand is cleaved from the corresponding precomplexes in catalytic alcohol amination reaction as confirmed by kinetic ^1H and ^{13}C NMR experiments as well as by X-ray characterization of intermediates and the catalyst resting state. We additionally confirmed that the different catalytic activities in organic solvents such as toluene as a function of the ligand or counterion reported recently, most probably originate from the different solubility of the catalysts in the organic medium. As expected, those differences are not present in media, which entirely dissolve the complexes, such as water. Despite of the decoordination of the aminoacidato ligands, we consider our precomplexes to be useful catalysts for alcohol amination because of the good solubility of some representatives both in organic solvents and in aqueous media, the mild reaction conditions, and the absence of activating additives.

EXPERIMENTAL SECTION

General Considerations. All manipulations were carried out in air using p. A. quality solvents, if not otherwise noted. Moisture and air sensitive reactions were performed under an anaerobic atmosphere of argon using standard Schlenk techniques. ^1H and ^{13}C NMR spectra were recorded on a Bruker Avance 200 MHz, 400 or 600 MHz spectrometer. ^1H and ^{13}C chemical shifts are reported relative to residual solvent signals of CD_2Cl_2 (5.32 ppm and 54.0 ppm), D_2O (4.79 ppm) or d_4-MeOD (3.31 ppm and 49.0 ppm). Multiplicities are reported as follows: *s* = singlet, *d* = doublet, *t* = triplet, *q* = quartet, *m* = multiplet. The ^{13}C NMR data was assigned by HSQC and HMBC spectra. FAB, ESI, and HR mass spectrometry was measured at the Mass Spectrometry Facility (Institute of the Organic Chemistry, University Heidelberg). Gas chromatography was performed on an Agilent 6890N modular GC base equipped with a split-mode capillary injection system and a flame ionization detector using a DB-1 capillary column (Agilent 122−1033; 30 m × 0.25 mm ×1.00 μm; He flow 1.0 mL/min, program: initial 70 °C for 5 min, ramp 5 °C/min, 300 °C for 10 min). Starting materials and products had following retention times: benzyl alcohol (t_R = 17.64 min), benzylamine (t_R = 16.93 min), dibenzylamine (t_R = 38.98 min), 1,6-hexanediol (t_R = 22.89 min), 1-benzylazepane (t_R = 33.69 min). Elemental analyses were performed in the "Mikroanalytisches Laboratorium der Chemischen Institute der Universität Heidelberg". For X-ray crystal structure analyses suitable crystals were mounted with a perfluorinated polyether oil on nylon loops or micro mounts and flash-frozen in a nitrogen stream at 200(2) K on the goniometer head. Data collection was performed with Mo−K_α radiation (λ = 0.71073 Å) from a Incoatec IμS microsource on a Bruker APEX-II diffractometer (**7**, **9**, **11**, **12**) or a sealed tube on a Bruker APEX diffractometer (**10**, **13**, **14**). 0.5° ω-scans were carried out to collect the intensity data in all cases. Intensities were corrected for Lorentz and polarization effects, and an empirical absorption correction was applied using SADABS[29] based on the Laue symmetry of the reciprocal space. The structures were solved by direct methods and refined against F^2 with a Full-matrix least-squares algorithm using the SHELXTL (Version 2008/4) software package.[30] Hydrogen atoms were treated using appropriate riding models, unless otherwise noted for the particular structures.

Table 2. Preparation of 1-Benzylazepane with Catalysts 2, 4, 6, 7, 10, 11, and 13 in Water

catalyst[a]	conv. (%)[b]	sel. (%)[c]
2	97	86
4	99	93
6	100	93
24[d]	100	90
7	96	93
10	99	85
11	100	83
13	97	89

[a]Conditions: $BnNH_2$ (2.5 mmol), 1,6-hexanediol (2.5 mmol), water (0.25 mL), cat. (2 mol %), 95 °C, 24 h, diglyme (0.5 mmol as standard). Conversion and selectivity determined by GC analysis. [b]Conversion in $BnNH_2$. [c]Selectivity in 1-benzylazepane. [d]$BnNH_2$ and **6** were stirred for 3 h at 20 °C prior to addition of 1,6-hexanediol to ensure the formation of Cp*Ir-amine adduct **24**.

*General Procedure for the Synthesis of Complexes **4** and **6**−**9**.* $[Cp^*IrCl_2]_2$ (**1**, 100 mg, 126 μmol) and amino acid (252

Scheme 6. Preparation of 1-Benzylazepane with Catalysts 2, 4, 6, 7, 10, 11, and 13 in Water[a]

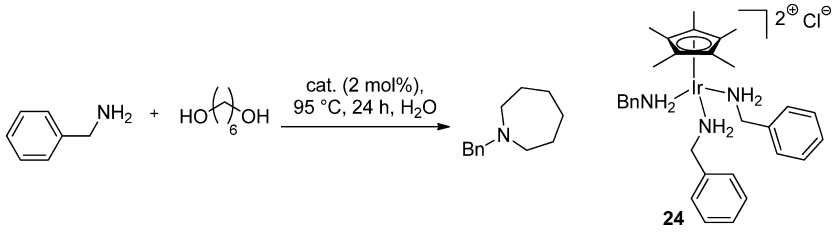

[a]For details, *cf.* Table 2.

dx.doi.org/10.1021/cs4009418 | ACS Catal. 2014, 4, 152−161

μmol, 2 equiv) were suspended in MeOH (15 mL). To this mixture was slowly added KO*t*Bu (265 μmol, 2.1 equiv) in MeOH (5 mL). The orange suspension turned into a homogeneous yellow solution at room temperature upon stirring (15−120 min). The solution was filtered, and the solvent was removed under reduced pressure. The yellow residue was retaken in acetone (15 mL), and the resulting suspension was filtered to remove KCl. The filtrate was again concentrated to dryness and the residue taken up in CH_2Cl_2 (2−3 mL), filtered over a pad of Celite, and the filter cake washed with CH_2Cl_2 (1−2 mL). The combined filtrates were layered with pentane (10−30 mL). After 1−2 d the yellow to orange crystals were collected by filtration (or decanting the solvent), washed with pentane, and dried in vacuum.

General Procedure for Mechanistic Studies. A high-pressure NMR tube was charged with [Cp*Ir(^{13}C,^{15}N-Gly)Cl] (**8**, 13.3 mg, 30 μmol) in d_8-toluene (0.5 mL). After measuring a blank sample (pure complex), 1-octanol (1 equiv, 4.75 μL, 30 μmol) was added, and the tube was pressurized with gaseous NH_3 (60 equiv). The tube was heated to 65 °C in an oil bath and regularly shaken to ensure proper mixing of the reaction mixture. NMR measurements were performed in regular intervals.

A high-pressure NMR tube was charged with [Cp*Ir(^{13}C,^{15}N-Gly)Cl] (**8**, 15.0 mg, 30 μmol) in D_2O (0.5 mL). After measuring a blank sample (pure complex), the tube was pressurized with gaseous NH_3 (10−60 equiv). NMR measurements were performed in regular intervals (TMS as external standard).

[Cp*Ir(Pro)Cl] (**4**).[12] 76.5 mg (160 μmol, 64% yield). − mp = 187 °C (decomp.); ^{1}H NMR (CD_2Cl_2, 600 MHz): δ = 1.65 (s, 15H, CH_3), 1.66−1.68 (m, 1H, CH_2), 1.89−1.97 (m, 2H, CH_2), 2.17−2.23 (m, 1H, CH_2), 2.90−2.97 (m, 1H, CH_2), 3.55−3.59 (m, 1H, CH_2), 3.89−3.93 (m, 1H, CH_2), 4.38 (bs, 1H, NH); ^{13}C NMR (CD_2Cl_2, 150 MHz): δ = 9.5 (CH_3), 27.7 (CH_2), 29.5 (CH_2), 55.3 (CH_2), 62.8 (CH), 84.7 (C_q), 184.1 (C_q).

[Cp*Ir(Gly)Cl] (**6**).[12] 74.6 mg (171 μmol, 68% yield). − mp = 236 °C (decomp.); ^{1}H NMR (d_4-MeOD, 600 MHz): δ = 1.70 (s, 15H, CH_3), 3.33−3.45 (m, 2H, CH_2); ^{13}C NMR (d_4-MeOD, 150 MHz): δ = 8.9 (CH_3), 45.7 (CH_2), 85.5 (C_q), 186.9 (C_q).

[Cp*Ir(Gly)I] (**7**). [Cp*IrI$_2$]$_2$ (**5**, 145 mg, 125 μmol) and glycine (19 mg, 250 μmol, 2 equiv) were suspended in MeOH (40 mL). To this mixture was slowly added KO*t*Bu (30 mg, 267 μmol, 2.1 equiv) in MeOH (5 mL). The orange suspension was stirred for 10 h at room temperature turning into a homogeneous yellow solution. After filtration, the solvent was evaporated and the residue redissolved in CH_2Cl_2 (6 mL), filtered over a pad of Celite, and layered with pentane (20−30 mL). A sequence of filtration and recrystallization from CH_2Cl_2 layered with excess pentane afforded 98.5 mg (186 μmol, 74% yield) of **7**. − mp =198 °C (decomp.); ^{1}H NMR (d_4-MeOD, 600 MHz): δ = 1.78 (s, 15H, CH_3), 3.40−3.46 (m, 2H, CH_2); ^{13}C NMR (d_4-MeOD, 150 MHz): δ = 9.7 (CH_3), 46.9 (CH_2), 86.4 (C_q), 186.8 (C_q); MS (FAB+): m/z = 530.0 [M+H]$^+$; Elemental analysis: Calcd. (%) for $C_{12}H_{19}IIrNO_2{\cdot}2CH_2Cl_2{\cdot}H_2O$: C 23.48, H 3.52, N 1.96. Found: C 23.28, H 3.57, N 2.09.

Yellow crystal (needle), dimensions 0.88 × 0.04 × 0.03 mm^3, crystal system monoclinic, space group $P2_1/c$, Z = 8, a = 9.0412(4) Å, b = 31.3975(15) Å, c = 12.3426(6) Å, α = 90°, β = 96.3560(10)°, γ = 90°, V = 3482.2(3) Å^3, ρ = 2.176 g/cm^3, Θ_{max} = 27.25°, covering the asymmetric unit in reciprocal space with a mean redundancy of 3.49 and a completeness of 99.9% to a resolution of 0.84 Å, 22826 reflections measured, 6889 unique (R(int) = 0.0475), 5235 observed ($I > 2\sigma(I)$). μ = 9.44 mm^{-1}, T_{min} = 0.04, T_{max} = 0.76, 380 parameters refined, goodness of fit 1.05 for observed reflections, final residual values R1(F) = 0.043, wR(F^2) = 0.072 for observed reflections, residual electron density −1.61−1.09 e Å^{-3}.

[Cp*Ir(^{13}C,^{15}N-Gly)Cl] (**8**). 98.5 mg (224 μmol, 89% yield). − mp =234 °C (decomp.); ^{1}H NMR (d_4-MeOD, 600 MHz): δ = 1.70 (s, 15H, CH_3), 3.35−3.43 (m, 2H, CH_2); ^{13}C NMR (d_4-MeOD, 150 MHz): δ = 8.9 (CH_3), 45.7 (dd, CH_2), 85.5 (C_q), 186.9 (d, C_q); MS (FAB): m/z = 440.1 [M+H]$^+$; Elemental analysis: Calcd. (%) for $C_{11}{}^{13}CH_{19}ClIr{}^{15}NO_2{\cdot}1/2CH_2Cl_2{\cdot}H_2O$: C 31.09, H 4.39, N 2.97. Found: C 31.25, H 4.32, N 2.99.

[Cp*Ir(Aib)Cl] (**9**). 101.5 mg (218 μmol, 87% yield). − mp >260 °C (decomp.); ^{1}H NMR (CD_2Cl_2, 400 MHz): δ = 1.33 (s, 3H, CH_3), 1.46 (s, 3H, CH_3), 1.69 (s, 15H, CH_3), 3.96 (d, 1H, $J_{H,H}$ = 10.5 Hz, NH_2), 4.72 (d, 1H, $J_{H,H}$ = 10.1 Hz, NH_2); ^{13}C NMR (CD_2Cl_2, 100 MHz): δ = 9.6 (CH_3), 27.5 (CH_3), 29.4 (CH_3), 58.1 (C_q), 84.6 (C_q), 184.8 (C_q); MS (FAB): m/z = 466.1 [M+H]$^+$; Elemental analysis: Calcd. (%) for $C_{14}H_{23}ClIrNO_2$: C 36.16, H 4.99, N 3.01. Found: C 36.23, H 5.06, N 2.90.

Yellow crystal (needle), dimensions 0.16 × 0.05 × 0.04 mm^3, crystal system triclinic, space group $P\bar{1}$, Z = 4, a = 9.1576(6) Å, b = 11.2916(8) Å, c = 16.2687(11) Å, α = 99.653(1)°, β = 91.159(1)°, γ = 91.704(1)°, V = 1657.2(2) Å^3, ρ = 1.864 g/cm^3, Θ_{max} = 31.06°, covering the asymmetric unit in reciprocal space with a mean redundancy of 3.83 and a completeness of 90.4% to a resolution of 0.69 Å, 36815 reflections measured, 9611 unique (R(int) = 0.0382), 7511 observed ($I > 2\sigma(I)$), μ = 8.22 mm^{-1}, T_{min} = 0.35, T_{max} = 0.73, 358 parameters refined, goodness of fit 1.03 for observed reflections, final residual values R1(F) = 0.034, wR(F^2) = 0.061 for observed reflections, residual electron density −1.16−2.74 e Å^{-3}.

[Cp*Ir(Gly)]$_3$(OTf)$_3$ (**10**). [Cp*Ir(Gly)Cl] (**6**, 160 mg, 380 μmol) was dissolved in CH_2Cl_2 (60 mL). To this solution was added AgOTf (97.6 mg, 380 μmol, 1.1 equiv), and the suspension was stirred for 2 h at 20 °C in the dark. The suspension was filtered over Celite, the solvent evaporated, and the pale yellow residue was redissolved in CH_2Cl_2. Diffusion of Et_2O into the complex solution afforded **10** as colorless crystals (167.3 mg, 101 μmol, 83% yield). − mp >260 °C (decomp.); ^{1}H NMR (d_4-MeOD, 200 MHz): δ = 1.77 (s, 45H, CH_3), 3.31 (d, 3H, CH_2), 3.77 (d, 3H, CH_2, $J_{H,H}$ = 17.5 Hz); ^{13}C NMR (CD_2Cl_2, 50 MHz): δ = 9.8 (CH_3), 46.2 (CH_2), 85.8 (C_q), 190.5 (C_q); MS (FAB): m/z = 402.0 [Cp*Ir(Gly)]$^+$; Elemental analysis: Calcd. (%) for $C_{39}H_{57}F_9Ir_3N_3O_{15}S_3$: C 28.36, H 3.48, N 2.54. Found: C 28.35, H 3.76, N 2.35.

Colorless crystal (polyhedron), dimensions 0.23 × 0.19 × 0.14 mm^3, crystal system orthorhombic, space group $P2_12_12_1$, Z = 4, a = 12.8738(18) Å, b = 16.382(2) Å, c = 26.730(4) Å, α = 90°, β = 90°, γ = 90°, V = 5637.4(14) Å^3, ρ = 2.014 g/cm^3, Θ_{max} = 29.51°, covering the asymmetric unit in reciprocal space with a mean redundancy of 7.64 and a completeness of 99.0% to a resolution of 0.72 Å, 62044 reflections measured, 15484 unique (R(int) = 0.1013), 13934 observed ($I > 2\sigma(I)$), μ = 7.27 mm^{-1}, T_{min} = 0.29, T_{max} = 0.43, 735 parameters refined, Flack absolute structure parameter −0.018(10), goodness of fit 1.02 for observed reflections, final residual values R1(F) = 0.050, wR(F^2) = 0.127 for observed reflections, residual electron density −1.69−2.52 e Å^{-3}.

dx.doi.org/10.1021/cs4009418 | *ACS Catal.* 2014, 4, 152−161

[Cp*Ir(Gly)MeCN]OTf (**11**). [Cp*Ir(Gly)Cl] (**6**, 114.7 mg, 260 μmol) was dissolved in MeCN (15 mL). To this solution was added AgOTf (74.2 mg, 290 μmol, 1.1 equiv) and the suspension stirred for 2 h at 20 °C in the dark. The suspension was filtered over Celite, the solvent evaporated, and the pale yellow residue was redissolved in MeCN. Diffusion of Et_2O in to the complex solution afforded **11** as yellow crystals (110.3 mg, 186 μmol, 71% yield). − mp >260 °C (decomp.); ^{1}H NMR (d_4-MeOD, 600 MHz): δ = 1.72 (s, 3H, CH_3CN), 1.77 (s, 15H, CH_3), 3.28 (d, 1H, CH_2, $J_{H,H}$ = 17.5 Hz), 3.77 (d, 1H, CH_2, $J_{H,H}$ = 17.5 Hz); ^{13}C NMR (d_4-MeOD, 150 MHz): δ = 9.1 (CH_3CN), 9.8 (CH_3), 46.2 (CH_2), 85.7 (C_q), 118.6, 120.7, 122.9, 125.0 (SO_3CF_3), 190.5 (C_q); the CN resonance is missing and might be hidden under the SO_3CF_3-resonance; MS (ESI, MeCN): m/z = 402.0 $[M\text{-MeCN-OTf}]^+$; Elemental analysis: Calcd. (%) for $C_{15}H_{22}F_3IrN_2O_5S$: C 30.45, H 3.75, N 4.74. Found: C 30.36, H 3.85, N 4.85.

Yellow crystal (polyhedron), dimensions 0.11 × 0.10 × 0.05 mm^3, crystal system monoclinic, space group $C2/c$, Z = 8, a = 26.456(2) Å, b = 8.5874(7) Å, c = 21.4517(18) Å, α = 90°, β = 121.888(1)°, γ = 90°, V = 4138.1(6) Å^3, ρ = 1.899 g/cm^3, Θ_{max} = 29.63°, covering the asymmetric unit in reciprocal space with a mean redundancy of 4.66 and a completeness of 100.0% to a resolution of 0.72 Å, 27855 reflections measured, 5827 unique (R(int) = 0.0458), 4618 observed ($I > 2\sigma(I)$), μ = 6.61 mm^{-1}, T_{min} = 0.53, T_{max} = 0.73, 250 parameters refined, goodness of fit 1.04 for observed reflections, final residual values R1(F) = 0.031, wR(F^2) = 0.056 for observed reflections, residual electron density −0.66−1.29 e Å^{-3}.

[Cp*Ir(Aib)NH$_3$]Cl (**12**). [Cp*Ir(Aib)Cl] (**9**, 32.7 mg, 70 μmol) was dissolved in MeOH (3 mL). To this solution was added NH_3 in water (15 M, 30 μL, 450 μmol, 6.4 equiv) and the solution was stirred for 1 h at 20 °C. The solvent was evaporated, and the residue solved in MeOH and filtered. Diffusion of Et_2O into the complex solution afforded **12** as yellow needles (20.4 mg, 42 μmol, 60% yield). − mp >233 °C (decomp.); ^{1}H NMR (d_4-MeOD, 600 MHz): δ = 1.38 (s, 3H, CH_3), 1.47 (s, 3H, CH_3), 1.74 (s, 15H, CH_3); ^{13}C NMR (d_4-MeOD, 150 MHz): δ = 9.0 (CH_3), 26.7 (CH_3), 27.8 (CH_3), 59.7 (C_q), 86.7 (C_q), 188.2 (C_q). Yellow crystal (needle), dimensions 0.15 × 0.04 × 0.03 mm^3, crystal system triclinic, space group $P\bar{1}$, Z = 2, a = 8.9727(6) Å, b = 10.0097(7) Å, c = 10.1814(7) Å, α = 75.441(1)°, β = 78.890(1)°, γ = 68.698(1)°, V = 819.37(10) Å^3, ρ = 1.954 g/cm^3, Θ_{max} = 30.62°, covering the asymmetric unit in reciprocal space with a mean redundancy of 3.73 and a completeness of 99.7% to a resolution of 0.70 Å, 18903 reflections measured, 5045 unique (R(int) = 0.0362), 4543 observed ($I > 2\sigma(I)$), μ = 8.31 mm^{-1}, T_{min} = 0.37, T_{max} = 0.79, 190 parameters refined, hydrogen atoms were treated using appropriate riding models, except at N2, where the hydrogen atoms were refined restrained, goodness of fit 1.05 for observed reflections, final residual values R1(F) = 0.024, wR(F^2) = 0.052 for observed reflections, residual electron density −0.86−1.36 e Å^{-3}.

[Cp*Ir(NH_3)$_3$]·2Cl (**13**).[10] ^{1}H NMR (d_4-MeOD, 200 MHz): δ = 1.75 (s, 15H, CH_3); ^{13}C NMR (d_4-MeOD, 50 MHz): δ = 8.4 (CH_3), 87.1 (C_q). Colorless crystal (polyhedron), dimensions 0.11 × 0.11 × 0.10 mm^3, crystal system monoclinic, space group $P21/c$, Z = 8, a = 10.3281(6) Å, b = 13.3359(7) Å, c = 24.1586(14) Å, α = 90°, β = 94.1269(14)°, γ = 90°, V = 3318.8(3) Å^3, ρ = 1.863 g/cm^3, Θ_{max} = 26.735°, covering the asymmetric unit in reciprocal space with a mean redundancy of 2.86 and a completeness of 99.6% to a resolution of 0.79 Å, 20464 reflections measured, 6723 unique (R(int) = 0.0372), 5673 observed ($I > 2\sigma(I)$), μ = 8.36 mm^{-1}, T_{min} = 0.44, T_{max} = 0.55, 325 parameters refined, goodness of fit 1.10 for observed reflections, final residual values R1(F) = 0.038, wR(F^2) = 0.073 for observed reflections, residual electron density −1.50−1.23 e Å^{-3}.

■ ASSOCIATED CONTENT

Supporting Information

NMR spectra of complexes, HR-FAB MS, and NMR data for selected reactions, computational details. This material is available free of charge via the Internet at http://pubs.acs.org. CCDC 962946 (**7**), 962947 (**9**), 962948 (**10**), 962949 (**11**), 962950 (**12**), 962951 (**13**), and 962952 (**14**) contain the supplementary crystallographic data for this paper. These data can be obtained free of charge from The Cambridge Crystallographic Data Centre via www.ccdc.cam.ac.uk/data_request/cif.

■ AUTHOR INFORMATION

Corresponding Author

*E-mail: michael.limbach@basf.com. Phone: +49-6216048957. Fax: +49-621606648957.

Notes

The authors declare no competing financial interest.

■ ACKNOWLEDGMENTS

S.W., P.P., P.H., and M.L. work at CaRLa of Heidelberg University, being cofinanced by Heidelberg University, the state of Baden-Württemberg, and BASF SE. Support from these institutions is gratefully acknowledged.

■ REFERENCES

(1) (a) Hesp, K. D.; Stradiotto, M. *ChemCatChem* **2010**, *2*, 1192−1207. (b) Oro, L. A.; Claver, C. *Iridium Complexes in Organic Synthesis*; Wiley-VCH: Weinheim, Germany, 2009; (c) Dobereiner, G. E.; Crabtree, R. H. *Chem. Rev.* **2009**, *110*, 681−703. (d) Cao, P.; Cabrera, J.; Padilla, R.; Serra, D.; Rominger, F.; Limbach, M. *Organometallics* **2012**, *31*, 921−929. (e) Lavy, S.; Miller, J. J.; Pažický, M.; Rodrigues, A.-S.; Rominger, F.; Jäkel, C.; Serra, D.; Vinokurov, N.; Limbach, M. *Adv. Synth. Catal.* **2010**, *352*, 2993−3000.

(2) (a) Berliner, M. A.; Dubant, S. P. A.; Makowski, T.; Ng, K.; Sitter, B.; Wager, C.; Zhang, Y. *Org. Process Res. Dev.* **2011**, *15*, 1052−1062. (b) Watson, A. J. A.; Maxwell, A. C.; Williams, J. M. J. *J. Org. Chem.* **2011**, *76*, 2328−2331.

(3) (a) Hamid, M. H. S. A.; Allen, C. L.; Lamb, G. W.; Maxwell, A. C.; Maytum, H. C.; Watson, A. J. A.; Williams, J. M. J. *J. Am. Chem. Soc.* **2009**, *131*, 1766−1774. (b) Bähn, S.; Tillack, A.; Imm, S.; Mevius, K.; Michalik, D.; Hollmann, D.; Neubert, L.; Beller, M. *ChemSusChem* **2009**, *2*, 551−557. (c) Gunanathan, C.; Milstein, D. *Angew. Chem., Int. Ed.* **2008**, *47*, 8661−8664. (d) Pingen, D.; Müller, C.; Vogt, D. *Angew. Chem., Int. Ed.* **2010**, *49*, 8130−8133.

(4) (a) Zhao, Y.; Foo, S. W.; Saito, S. *Angew. Chem., Int. Ed.* **2011**, *50*, 3006−3009. (b) He, L.; Lou, X.-B.; Ni, J.; Liu, Y.-M.; Cao, Y.; He, H.-Y.; Fan, K.-N. *Chem.—Eur. J.* **2010**, *16*, 13965−13969. (c) Bähn, S.; Imm, S.; Neubert, L.; Zhang, M.; Neumann, H.; Beller, M. *ChemCatChem* **2011**, *3*, 1853−1864.

(5) (a) Andrushko, N.; Andrushko, V.; Roose, P.; Moonen, K.; Börner, A. *ChemCatChem* **2010**, *2*, 640−643. (b) da Costa, A. P.; Sanau, M.; Peris, E.; Royo, B. *Dalton Trans.* **2009**, 6960−6966. (c) Pontes da Costa, A.; Viciano, M.; Sanaú, M.; Merino, S.; Tejeda, J.; Peris, E.; Royo, B. *Organometallics* **2008**, *27*, 1305−1309. (d) Cami-Kobeci, G.; Williams, J. M. J. *Chem. Commun.* **2004**, 1072−1073. (e) Tanaka, N.; Hatanaka, M.; Watanabe, Y. *Chem. Lett.* **1992**, *21*, 575−578. (f) Suzuki, T. *Chem. Rev.* **2011**, *111*, 1825−1845.

(6) (a) Fujita, K.-i.; Enoki, Y.; Yamaguchi, R. *Tetrahedron* **2008**, *64*, 1943−1954. (b) Fujita, K.-i.; Yamaguchi, R. *Synlett* **2005**, *2005*, 560−571. (c) Fujita, K.-i.; Fujii, T.; Yamaguchi, R. *Org. Lett.* **2004**, *6*, 3525−3528. (d) Fujita, K.-i.; Li, Z.; Ozeki, N.; Yamaguchi, R. *Tetrahedron Lett.* **2003**, *44*, 2687−2690. (e) Fujita, K.-i.; Yamamoto, K.; Yamaguchi, R. *Org. Lett.* **2002**, *4*, 2691−2694.
(7) Gnanamgari, D.; Sauer, E. L. O.; Schley, N. D.; Butler, C.; Incarvito, C. D.; Crabtree, R. H. *Organometallics* **2009**, *28*, 321−325.
(8) Prades, A.; Corberán, R.; Poyatos, M.; Peris, E. *Chem.—Eur. J.* **2008**, *14*, 11474−11479.
(9) (a) Blank, B.; Michlik, S.; Kempe, R. *Chem.—Eur. J.* **2009**, *15*, 3790−3799. (b) Sakaguchi, S.; Yamaga, T.; Ishii, Y. *J. Org. Chem.* **2001**, *66*, 4710−4712.
(10) Kawahara, R.; Fujita, K.-i.; Yamaguchi, R. *J. Am. Chem. Soc.* **2010**, *132*, 15108−15111.
(11) Kawahara, R.; Fujita, K.-i.; Yamaguchi, R. *Adv. Synth. Catal.* **2011**, *353*, 1161−1168.
(12) Wetzel, A.; Wöckel, S.; Schelwies, M.; Brinks, M. K.; Rominger, F.; Hofmann, P.; Limbach, M. *Org. Lett.* **2013**, *15*, 266−269.
(13) (a) Koch, D.; Sünkel, K.; Beck, W. *Z. Anorg. Allg. Chem.* **2003**, *629*, 1322−1328. (b) Carmona, D.; Lamata, M. P.; Viguri, F.; San José, E.; Mendoza, A.; Lahoz, F. J.; García-Orduña, P.; Atencio, R.; Oro, L. A. *J. Organomet. Chem.* **2012**, *717*, 152−163. (c) Jimeno, M. L.; Elguero, J.; Carmona, D.; Lamata, M. P.; San José, E. *Magn. Reson. Chem.* **1996**, *34*, 42−46. (d) Poth, T.; Paulus, H.; Elias, H.; Dücker-Benfer, C.; van Eldik, R. *Eur. J. Inorg. Chem.* **2001**, *2001*, 1361−1369. (e) Carmona, D.; Vega, C.; Lahoz, F. J.; Atencio, R.; Oro, L. A.; Lamata, M. P.; Viguri, F.; San José, E. *Organometallics* **2000**, *19*, 2273−2280. (f) Carmona, D.; Lahoz, F. J.; Atencio, R.; Oro, L. A.; Lamata, M. P.; San José, E. *Tetrahedron: Asymmetry* **1993**, *4*, 1425−1428. (g) Grotjahn, D. B.; Groy, T. L. *J. Am. Chem. Soc.* **1994**, *116*, 6969−6970. (h) Grotjahn, D. B.; Groy, T. L. *Organometallics* **1995**, *14*, 3669−3682. (i) Carmona, D.; Mendoza, A.; Lahoz, F. J.; Oro, L. A.; Lamata, M. P.; San Jose, E. *J. Organomet. Chem.* **1990**, *396*, C17−C21. (j) Krämer, R.; Polborn, K.; Wanjek, H.; Zahn, I.; Beck, W. *Chem. Ber.* **1990**, *123*, 767−778.
(14) Koch, D.; Hoffmüller, W.; Polborn, K.; Beck, W. *Z. Naturforsch.* **2001**, *56b*, 403−410.
(15) Hoffmüller, W.; Dialer, H.; Beck, W. *Z. Naturforsch.* **2005**, *60b*, 1278−1286.
(16) Carmona, D.; Lahoz, F. J.; Atencio, R.; Oro, L. A.; Lamata, M. P.; Viguri, F.; San José, E.; Vega, C.; Reyes, J.; Joó, F.; Kathó, Á. *Chem.—Eur. J.* **1999**, *5*, 1544−1564.
(17) White, C.; Yates, A.; Maitlis, P. M.; Heinekey, D. M. *Inorg. Synth.* **2007**, 228−234.
(18) Stirling, M.; Blacker, J.; Page, M. I. *Tetrahedron Lett.* **2007**, *48*, 1247−1250.
(19) Sünkel, K.; Hoffmüller, W.; Beck, W. *Z. Naturforsch.* **1998**, *53b*, 1365−1368.
(20) (a) Becke, A. D. *J. Chem. Phys.* **1993**, *98*, 5648−5632. (b) Grimme, S.; Antony, J.; Ehrlich, S.; Krieg, H. *J. Chem. Phys.* **2010**, *132*, 154104−1−154104−19. (c) Zhao, Y.; Truhlar, D. G. *Theor. Chem. Acc.* **2008**, *120*, 215−241. (d) Schäfer, A.; Huber, C.; Ahlrichs, R. *J. Chem. Phys.* **1994**, *100*, 5829−5835.
(21) (a) Dirac, P. A. M. *Proc. R. Soc. (London) A* **1929**, *123*, 714−733. (b) Becke, A. *Phys. Rev. A* **1988**, *38*, 3098−3100. (c) Perdew, J. P.; Wang, Y. *Phys. Rev. B* **1992**, *45*, 13244−13249. (d) Vosko, S. H.; Wilk, L.; Nusair, M. *Can. J. Phys.* **1980**, *58*, 1200−1211. (e) Perdew, J. P. *Phys. Rev. B* **1986**, *33*, 8822−8824. (f) Schäfer, A.; Horn, H.; Ahlrichs, R. *J. Chem. Phys.* **1992**, *97*, 2571−2577.
(22) (a) Eichkorn, K.; Treutler, O.; Ohm, H.; Haser, M.; Ahlrichs, R. *Chem. Phys. Lett.* **1995**, *242*, 652−660. (b) Eichkorn, K.; Weigend, F.; Treutler, O.; Ahlrichs, R. *Theor. Chem. Acc.* **1997**, *97*, 119−124. (c) Weigend, F. *Phys. Chem. Chem. Phys.* **2006**, *8*, 1057−1065.
(23) TURBOMOLE V6.4 2012, a development of University of Karlsruhe and Forschungszentrum Karlsruhe GmbH, 1989−2007, TURBOMOLE GmbH, since 2007; available from http://www.turbomole.com.
(24) (a) Marenich, A. V.; Cramer, C. J.; Truhlar, D. G. *J. Phys. Chem. B* **2009**, *113*, 6378−6396. (b) Schmidt, M. W.; Baldridge, K. K.; Boatz, J. A.; Elbert, S. T.; Gordon, M. S.; Jensen, J. H.; Koseki, S.; Matsunaga, N.; Nguyen, K. A.; Su, S.; Windus, T. L.; Dupuis, M.; Montgomery, J. A. *J. Comput. Chem.* **1993**, *14*, 1347−1363. (c) Feller, D. *J. Comput. Chem.* **1996**, *17*, 1571−1586. (d) Schuchardt, K. L.; Didier, B. T.; Elsethagen, T.; Sun, L.; Gurumoorthi, V.; Chase, J.; Li, J.; Windus, T. L. *J. Chem. Inf. Model.* **2007**, *47*, 1045−1052. (e) Eckert, F.; Klamt, A. *COSMOtherm*, Version C3.0, Release 12.01; COSMOlogic GmbH & Co KG: Leverkusen, Germany, 2012. (f) Eckert, F.; Klamt, A. *AIChE J.* **2002**, *48*, 369−385.
(25) Tissandier, M. D.; Cowen, K. A.; Feng, W. Y.; Gundlach, E.; Cohen, M. J.; Earhart, A. D.; Coe, J. V. *J. Phys. Chem. A* **1998**, *102*, 7787−7794.
(26) Jones, F. M.; Arnett, E. M. *Prog. Org. Chem.* **1974**, *11*, 263−322.
(27) Ward, T. R.; Schafer, O.; Daul, C.; Hofmann, P. *Organometallics* **1997**, *16*, 3207−3215.
(28) The highest catalyst activity and selectivity to the secondary amine for the reaction of BnOH with aniline catalyzed by **6** (2 mol%, 140 °C, 24 h) was found in toluene (toluene: 94% conv, 96% sel; *o*-xylene: 96% conv, 53% sel; diethyleneglycol: 79% conv, 91% sel; neat: 99% conv, 93% sel to the tertiary amine).
(29) , Sheldrick, G. M. *SADABS 2008/1, Program for absorption correction*; Bruker Analytical X-ray-Division: Madison, WI, 2008.
(30) Software package SHELXTL 2008/4 for structure solution and refinement; Sheldrick, G. M. *Acta Crystallogr.* **2008**, *A64*, 112−122.